https://doi.org/10.5194/egusphere-2026-3049
Preprint. Discussion started: 3 June 2026

Seasonal evolution of suncup roughness describes broadband albedo decay on alpine snow

Francesca Carletti[1,2], Nora Helbig[1], Nander Wever[1], Loïc Brouet[1], Mathias Bavay[1], Benjamin Walter[1], and Michael Lehning[1,2]

[1]WSL Institute for Snow and Avalanche Research SLF, Davos Dorf, Switzerland
[2]School of Architecture, Civil and Environmental Engineering, École Polytechnique Fédérale de Lausanne EPFL, Lausanne, Switzerland

Correspondence: Francesca Carletti (francesca.carletti@slf.ch)

Abstract. We monitored the formation and seasonal evolution of suncup roughness over three snow ablation seasons at Weissfluhjoch, Swiss Alps, using a terrestrial LiDAR scanner. Suncup onset required two concurrent conditions, identified from high-temporal-resolution digital surface models of surface roughness: sustained surface melting through most of the day and reduced wind speeds. Suncups formed in all three years, but their planar arrangement and geometric properties varied substantially across seasons, controlled by whether radiative or turbulent heat exchange dominated ablation. Comparing measured broadband albedo to flat-surface simulations from TARTES forced by SNOWPACK-modelled snow properties, we find that the combined effect of suncup roughness and surface impurity loading reduces albedo by 0.02–0.15, depending on illumination geometry and impurity load, consistent with previous literature. Isolating the two contributions is complicated by their co-evolution during the ablation season: the same melt processes that progressively deepen suncups also drive surface enrichment and spatial redistribution of impurities. Resolving the two effects independently would in principle require equally fine-scale measurements of both roughness and impurity distribution. We identify a robust logarithmic correlation between broadband albedo and aerodynamic roughness length that simultaneously captures the radiative effects of roughness and impurities, regardless of their relative contributions. During early suncup formation, impurities remained uniformly distributed. At later stages, meltwater scavenging concentrated impurities to the suncup hollows. As the rate of broadband albedo decay is strongest at the beginning of suncup formation and relaxes thereafter, we infer that the interaction between the multiple-reflection mechanism and the more uniform distribution of impurities is particularly effective in accelerating albedo decay, beyond the effect of either factor alone. Given that C-band SAR backscatter is sensitive to the early development of surface roughness on wet snow, these findings encourage future work on the assimilation of surface roughness into snow energy balance models.

1 Introduction

Snow is the most reflecting natural surface on Earth, scattering up to 98% of incident solar radiation in its pristine state (Wiscombe and Warren, 1980). Therefore, even marginal decreases in albedo substantially increase the proportion of absorbed solar energy. Because seasonal snow can cover up to the 50% of the Northern Hemisphere each year (Armstrong and Brodzik,

https://doi.org/10.5194/egusphere-2026-3049
Preprint. Discussion started: 3 June 2026

2001), even small albedo reductions have large effects on the Earth's energy budget (Flanner et al., 2011). Several factors determine albedo decreases in snow, and they often concur in a complex way: snow metamorphism reducing the specific surface area (SSA) of the grains (Wiscombe and Warren, 1980; Domine et al., 2006), the grain shape (Robledano et al., 2023; Libois et al., 2014, 2013), the presence of liquid water at the surface (Dumont et al., 2017), the incident angle (Warren, 1982), the concentration of light-absorbing particles (LAPs; Skiles et al. (2018)), and the presence of surface roughness features (Warren et al., 1998; Zhuravleva and Kokhanovsky, 2011). Surface roughness received less attention than other albedo drivers, partly because it is very heterogeneous across spatial scales (Fassnacht et al., 2023), making it difficult to identify the scale most relevant to the radiative footprint of the measuring sensor. Yet, since snow surfaces are rarely flat, roughness is the primary physical cause of the divergence between intrinsic albedo (i.e., the bihemispherical reflectance of a substance, Schaepman-Strub et al. (2006)) and apparent albedo (i.e., the ratio of reflected to incident radiation). In the context of surface energy balance, the apparent albedo is the physically meaningful quantity, since pyranometer-based measurements inherently integrate the effects of surface roughness within their radiative footprint (Bair et al., 2016, 2015).

In the accumulation phase, macroscopic surface roughness features such as sastrugi, ripples, and dunes often result from snow transport or erosion by wind (Sommer et al., 2018; Amory et al., 2017; Filhol and Sturm, 2015). Many studies showed systematic albedo decreases in presence of such features (Corbett and Su, 2015; Leroux and Fily, 1998; Carroll, 1982), which can reach several meters in height (Warren et al., 1998). In the ablation phase, at high-altitude, arid environments where snow ablation is driven by sublimation rather than melting, snow penitentes form (Betterton, 2001; Lliboutry, 1954). They appear as snow pillars pointing towards the sun potentially reaching several meters in height, and cause apparent albedo to drop by up to 0.4 (Lhermitte et al., 2014; Corripio and Purves, 2005). Penitentes do not form in the Alps under current climatic conditions, where humidity is too high and melting dominates over sublimation. However, high-alpine snowfields at mid-latitudes develop their own characteristic ablation roughness features in the form of ablation hollows, more commonly referred to as suncups. Suncups show up as a quasi-periodic natural pattern composed of round, concave dimples that can grow vertically and laterally by up to tenths of centimeters, separated by rounded ridges (Betterton, 2001; Rhodes et al., 1987; Matthes, 1934). According to Betterton (2001); Lliboutry (1954), suncups are early forms of penitentes, sharing the same initial instability mechanism, i.e. radiation clustering in concavities creating a positive feedback that deepens the hollows.

The albedo decay over a rough snow surface is controlled by two mechanisms that activate under different illumination conditions: (1) the effective-angle effect and (2) multiple reflections in the hollows (Warren et al., 1998). The effective-angle refers to a simultaneous effect of surface features facing the sun and away from the sun. The former receive solar radiation at a smaller incidence angle than the solar zenith angle, causing stronger absorption; the latter are either shadowed or only illuminated at grazing angles and therefore contribute marginally to the total reflected flux. The insolation-weighted albedo of a rough surface is therefore reduced with respect to that of a flat surface under equivalent illumination conditions (Kokhanovsky and Zege, 2004; Warren et al., 1998; Warren, 1982). This effect varies with shape and orientation of the roughness features (Larue et al., 2020; Lhermitte et al., 2014) and only activates in conditions of direct illumination and larger solar zenith angles (Warren et al., 1998). The multiple reflections effect activates because, on a rough surface, the probability of photons being trapped inside concavities rather than being scattered away is higher than it is for a flat surface. After each collision with the

https://doi.org/10.5194/egusphere-2026-3049
Preprint. Discussion started: 3 June 2026

roughness walls, the probability of light being absorbed rather than reflected increases. This causes a systematic increase in absorption, especially in conditions where reflection and absorption are balanced, i.e., for values of albedo close to 0.5 in the near-infrared (NIR, 700-1100 nm) (Bair et al., 2022; Larue et al., 2020). This effect is active under both direct and diffuse illumination conditions.

As an alpine snowpack melts, its surface is simultaneously rugged by suncup growth and progressively darkened by the enrichment of LAPs such as black carbon or mineral dust. LAPs are fundamental drivers of albedo reductions (Warren and Wiscombe, 1980) both directly, as they enhance solar energy absorption in the visible range (400-700 nm), and indirectly, as they accelerate near-surface SSA decrease that further decreases albedo (Skiles and Painter, 2019; Tuzet et al., 2017). Specifically, as the snow melts, black carbon and dust are retained at the snow surface because the scavenging efficiency of percolating meltwater is less than 100%, causing surface concentrations to increase by up to a factor of 5 during extreme melt events, an effect referred to as melt amplification (Doherty et al., 2013; Conway et al., 1996). Moreover, in late spring, algal populations of *Sanguina nivaloides* can proliferate quickly and form red blooms near the snow surface (Stewart et al., 2021). Algae reduce the albedo of snow surfaces similarly to LAPs, but unlike LAPs, their proliferation depends on specific environmental conditions and it is not a systematic feature of snowmelt. In their recent work, Roussel et al. (2024) demonstrated that proliferation of *S. nivaloides* requires a snowmelt duration exceeding 46 days and is unlikely when the ground beneath the snowpack is frozen. The authors further suggest that nutrients supplied by Saharan dust may also drive algal blooms.

Isolating the effect of suncups on albedo is therefore not straightforward, particularly as the environmental conditions governing suncup development, melt amplification, and algal proliferation vary between seasons, complicating the derivation of general conclusions. In experiments with artificially modified snow surface roughness, Larue et al. (2020) disentangled and quantified the effective-angle and multiple reflections effects, introduced above. They found that roughness reduced albedo by up to 0.1 at 1000 nm, that both effects are amplified when SSA is low (<10 m^2kg^{-1}), and that the effective-angle effect enhances rapidly at large solar zenith angles. Manninen et al. (2021) and Bair et al. (2022) validated the framework of Larue et al. (2020) on natural snow roughness: a surface that, in case of suncups, would be almost impossible to replicate artificially. Importantly, Larue et al. (2020) did not account for the concomitant effect of LAPs. Manninen et al. (2021) monitored roughness, broadband albedo and spectral reflectance in Finnish Lapland for a total of 3 months over two years. They showed how centimeter-scale surface roughness comparable to that of suncups decreased the broadband albedo by 0.1 during the late melting season, especially for smaller solar zenith angles and lower bulk albedo values. To date, the most temporally extensive study was carried out by Bair et al. (2022) in Sierra Nevada: the surface was tracked for roughly 100 days with a LiDAR system and field spectroradiometry to simultaneously track suncup growth, resolve grain size and impurity content, and quantify the resulting albedo reduction (0.05 in the broadband). Moreover, Bair et al. (2022) found a major challenge associated with multispectrometry. Because for multispectral sensors pixels containing mixed fractions of pristine and dirty snow are spectrally inseparable from pixels containing only dirty snow, urface roughness effects on albedo cannot be separated from impurity effects, unless the snow is relatively dirty. Similar conclusions were reached by Warren (2013). With suncup roughness driving differential dirt concentration between hollows, ridges, and walls (Rhodes et al., 1987; Takahashi, 1978; Jahn and Kłapa, 1968;

https://doi.org/10.5194/egusphere-2026-3049
Preprint. Discussion started: 3 June 2026

Richardson and Harper, 1957), a suncup field presents a spatially heterogeneous mix of clean and dirty snow at the sub-pixel scale, potentially rendering all pixels as mixed for a multispectral sensor.

Spectral albedo measurements provide richer information than broadband, as they enable the attribution of surface albedo changes, i.e., the reflectivity of the snow surface, to snow microstructure (Libois et al., 2013), liquid water (Dumont et al., 2017), impurities (Tuzet et al., 2019; Skiles et al., 2018), or algae (Roussel et al., 2024; Painter et al., 2001). However, spectral measurements require expensive instrumentation and are particularly labor-intensive (e.g. Donahue et al. (2022)), making them impractical for unsupervised, continuous deployment at high-alpine sites; as a consequence, they are carried out sporadically. Broadband pyranometers, conversely, are simpler, more robust, and better suited for long-term unattended deployment in harsh environments, enabling continuous monitoring at high temporal resolution across multiple melt seasons. This makes broadband measurements better suited for capturing inter-annual variability in surface conditions. Furthermore, as most physically based snowpack models use broadband albedo as a target variable, improving the understanding of how surface roughness affects broadband albedo has direct relevance for snowmelt modelling. In particular, Carletti et al. (2025) recently showed that Sentinel-1 backscatter is especially sensitive to the early development of surface roughness on wet snow; characterizing its relationship with broadband albedo is therefore essential for the design of assimilation schemes.

Here we present the first three-season survey of suncup roughness on high-altitude alpine snow during the ablation phase. We characterise the conditions governing suncup onset and the inter-annual variability in planar arrangement and geometric properties as a function of measurable snow state variables and meteorological forcing. We then compare broadband albedo measurements to smooth-surface TARTES simulations under pristine and impurity-loaded conditions, using scenarios of impurity content based on existing alpine surveys, and apply the effective albedo parametrization of Löwe and Helbig (2012) to account for suncup-induced albedo reductions. We address the challenge posed by the co-evolution of suncup growth and progressive impurity concentration and clustering at the snow surface, which complicates the separation of their individual contributions to albedo decay, and propose a practical way forward based on the empirical relationship between measured broadband albedo and aerodynamic roughness length. Together, these results motivate and assist the explicit representation of ablation-driven surface roughness in snow energy balance models.

2 Data and Methods

2.1 Surface microtopographies and roughness indices

LiDAR laser scanning is an established effective technique to monitor surface roughness (Bair et al., 2022; Lacroix et al., 2008) and a wide variety of snow processes in general (e.g. Ruttner et al. (2025)). A fixed, automated, high-resolution 3D Terrestrial Laser Scanner (TLS; FARO® Focus3D S120) scanned a delimited area of about 300 m^2 in the immediate proximity of the Weissfluhjoch research station (2536 m a.s.l., Davos, Switzerland), at hourly resolution and over three snow seasons. The TLS occasionally required restarting or relocation, resulting in mostly minor data gaps, the largest occurring in 2023, when the TLS only became operational in April and no acquisitions were made beforehand. Moreover, less than 2% of the scans were discarded due to acquisition instabilities caused by wind gusts or heavy snowfall. Because the scanned area is large

https://doi.org/10.5194/egusphere-2026-3049
Preprint. Discussion started: 3 June 2026

and contains obstacles such as instruments and fences, and because point density decreases with distance from the scanner due to decreasing incidence angle, the point clouds were reduced to a region of interest (ROI) of ∼10 x ∼4 m. The ROI is then projected to the horizontal plane. To remove points not belonging to the snow surface (be it snowflakes from snowfall or blowing snow, or random noise) which would disturb the interpolation, we applied the well-established cloth simulation filtering algorithm of Zhang et al. (2016), with a cloth resolution of 30 cm, a classification threshold of 10 cm and maximum rigidness, as recommended for flat terrain. On average, 1% of the points per scan were filtered out. The filtered point clouds were then interpolated to a regular grid of 5 mm resolution using bilinear interpolation to produce digital surface models (DSMs). Ultimately, the altitude trend was removed using Gaussian filtering, unraveling the microtopographic reliefs and concavities. The result is a time series of microtopographic DSMs, suitable for the estimation of surface roughness indices using raster approaches (Fassnacht et al., 2009).

We computed surface roughness indices across two complementary scales. Vertical indices characterize the amplitude of surface reliefs; to represent it, we chose the root mean square of heights (RMSH) and the aerodynamic roughness length (z_0), computed with the raster-based version of Lettau (1969). The root mean square of heights measures the standard deviation of a surface's height deviations relative to a flat mean plane (Manninen, 2003, 1997). The aerodynamic roughness length is the theoretical height above a surface at which the mean wind speed logarithmic profile extrapolates to zero (Lettau, 1969). Horizontal indices, on the other hand, characterize the lateral scale of the surface reliefs; to represent it, we chose the correlation length (CL). Correlation length expresses the horizontal distance over which surface height fluctuations remain statistically correlated, i.e., the scale beyond which two points on the surface can be considered uncorrelated with respect to their elevation (Manninen, 2003, 1997). These metrics inform differently on the state of the snow surface. A sastrugi field, for example, is characterized by high horizontal and moderate-low vertical roughness indices: reliefs are often spatially extended and spaced far apart. Suncups, conversely, show low horizontal and high vertical roughness indices, as reliefs of similar amplitude arrange periodically over short distances. Moreover, we computed raster-based descriptors of suncup formation and growth through image analysis of the DSMs, such as the number of features with a negative height, the mean planar extension, the mean depth, and the 2D equivalent of the roughness coverage fraction η used in Larue et al. (2020). Unlike in Larue et al. (2020), the non-concave portions of our natural surfaces are not flat; therefore, ridges were incorporated into the calculation.

2.2 SNOWPACK simulations of snowpack state variables

Snow metamorphism decreases albedo through changes in snow density, liquid water content, and SSA. We simulated the evolution of these snowpack properties with SNOWPACK (Bartelt and Lehning, 2002), a 1D multi-layer snow physical model describing a complete ensemble of processes that impact the snow energy balance, such as metamorphism and microstructure (Vionnet et al., 2012; Lehning et al., 2002), phase changes, liquid water transport and preferential flow (Würzer et al., 2017; Wever et al., 2016, 2014), and turbulent kinetic exchanges at the surface (Schlögl et al., 2018) among others. We forced the snow surface temperature as a Dirichlet upper boundary condition as long as the snow surface was in sub-freezing conditions and used calculated energy fluxes as Neumann boundary conditions during melt. SNOWPACK simulations were forced with quality-controlled measurements from advanced meteorological sensors at the research station and its immediate surroundings.

https://doi.org/10.5194/egusphere-2026-3049
Preprint. Discussion started: 3 June 2026

Table 1. Impurity concentration scenarios.

Scenario	Black carbon [ng g^{-1}]	Dust [µg g^{-1}]	*S. nivaloides* [µg g^{-1}]	Reference(s)
Pristine	0	0	0	
Low	40	10	0	Tuzet et al. (2020); Kau et al. (2026); Gabbi et al. (2015); Di Mauro et al. (2019)
Medium	80	50	0	Tuzet et al. (2020); Kau et al. (2026); Gabbi et al. (2015); Di Mauro et al. (2019)
High	200	100	0	Doherty et al. (2013)
Algae	0	0	66	Roussel et al. (2024); Chevrollier et al. (2023)

The SNOWPACK output includes energy fluxes and full profiles of snow temperature, density and optical grain size among others, at a sub-hourly and 3-hour resolution, respectively. Such information is combined with the nearest acquisition of surface roughness in time.

The ability of SNOWPACK to reproduce SSA and density of individual layers at Weissfluhjoch was thoroughly investigated by Calonne et al. (2020). Over one winter season, the authors indicate overall SSA underestimations from SNOWPACK, with the amplitude of the deviations depending on the compared measurement technique. With respect to densities, Calonne et al. (2020) pointed out that SNOWPACK overestimates the densification rate of lower snowpack layers and, conversely, underestimates the density of surface layers evolving from fresh snow to rounded grains.

2.3 TARTES simulations of broadband albedo

We used the Two-streAm Radiative TransfEr in Snow (TARTES; Picard and Libois (2024)) to simulate the spectral albedo (350-2200nm) of a flat snowpack, with density and optical grain size prescribed by SNOWPACK. Because incident light is either absorbed or back-scattered by snow grains within 10 to 20 cm from the snow surface (Kokhanovsky, 2022; Libois et al., 2013), we prescribed numerical layers 1 cm thick for the top 10 cm, and a single layer of weighed averaged properties below. For each layer, the type and concentration of impurities has to be prescribed.

As impurity content measurements were unavailable at our site, we designed three scenarios (Tab. 1) building upon the existing monitoring campaigns in the Alps, assuming that LAPs absorption is only attributable to black carbon and dust (Tuzet et al., 2020). Specifically, our medium black carbon scenario matches the observed maxima in the two-year campaign of Tuzet et al. (2020) and is consistent with several previous assessments (see Tab. 1). Our high black carbon scenario reflects extreme melt events where the surface concentration can multiply through melt amplification (Doherty et al., 2013). Our dust scenarios are based upon the measurements and simulations of Di Mauro et al. (2019), considering Algeria as the main source area of Saharan dust ($PM_{2.5}$) reaching Europe. TARTES computes the mass absorption efficiency of impurities assuming optical properties for black carbon (Bond and Bergstrom, 2006) and dust (Caponi et al., 2017).

The optical properties of red snow algae are not implemented in the current version of TARTES. Therefore, we incorporated them as a custom light-absorbing impurity using the empirical *in vivo* properties measured by Chevrollier et al. (2023). For the algal bloom scenario, we estimated a mass mixing ratio from the minimum cell concentration detectable by Sentinel-2 (∼20000 cells/ml; Roussel et al. 2024), representing bloom intensities with a measurable impact on the surface reflectance;

https://doi.org/10.5194/egusphere-2026-3049
Preprint. Discussion started: 3 June 2026

a cell dry mass of 10^{-12} kg/cell derived from the mean snow algal biovolume and dry density reported in Chevrollier et al. (2023), and the mean modelled snow surface density during the melt season (300 kgm^{-3}); yielding a mass mixing ratio of 66 $\mu g g^{-1}$.

We ran TARTES simulations in diffuse (cloudy/overcast-sky) and direct (clear-sky) conditions and compared them with measurements from a Kipp&Zonen CM21 broadband pyranometer. Using the formulation of Picard et al. (2020) to compute the ratio r_λ between incoming diffuse and global horizontal irradiance, we classified timesteps with $r_\lambda \leq 0.2$ as direct-dominated and $r_\lambda \geq 0.95$ as diffuse-dominated. The deliberately wide gap between thresholds likely excludes mixed illumination conditions, ensuring each group represents a quasi-pure illumination condition. In absence of a separate diffuse radiation sensor, the diffuse fraction was obtained from decomposing measured global radiation using the formulations of Helbig et al. (2010); Tapakis et al. (2015); Reindl et al. (1990) implemented in MeteoIO (Bavay and Egger, 2014), SNOWPACK's meteorological preprocessing library. Moreover, for direct illumination conditions, measurements with solar zenith angles exceeding 60° were excluded to avoid sensor's cosine response errors (Grenfell et al., 1994). Modelled broadband albedo values for both illumination conditions are obtained by weighting the TARTES spectral albedo by modelled incident solar spectra for clear and overcast skies (Dadic et al., 2013).

2.4 Effective albedo parametrization

To (partially) account for the effect of suncup roughness on the domain-averaged broadband albedo, we applied the effective albedo parametrization presented in Löwe and Helbig (2012), originally formulated for subgrid topographic shading in large-scale models, but fully applicable to smaller scales to the first order, provided the surface statistics are described by the same geometric parameters. These parameters are, in fact, the mean-squared slope μ and the sky-view factor ψ. According to these parameters, this approach modifies the flat-surface albedo computed by TARTES. Specifically, the direct irradiance is attenuated by a shading factor that accounts for the fraction of the surface in shadow as a function of the solar zenith angle and μ, including partial shadowing at low sun elevations when suncup walls shade adjacent terrain. The diffuse irradiance is reduced in proportion to ψ, whereas the obstructed fraction $(1 - \psi)$ adds up the terrain-reflected radiation. Both μ and ψ were derived from the LiDAR surface scans.

As the shading factor depends on solar zenith angle and decreases significantly under diffuse illumination (cloudy/overcast sky), direct-dominated illumination conditions are where shading between suncup walls is the dominant roughness-induced albedo reduction mechanism (Larue et al., 2020). Under overcast sky, the remaining roughness-induced albedo reductions are instead governed by the limited sky view factor and single terrain reflections, both of which are included in the parameterization. Multiple reflections are not accounted for under either condition in the parametrization of Löwe and Helbig (2012). This practical compromise is motivated by the need for a quasi-analytical method that can be applied systematically across three seasons of hourly LiDAR roughness acquisitions, where full 3D ray-tracing would result in extreme computational complexity.

https://doi.org/10.5194/egusphere-2026-3049
Preprint. Discussion started: 3 June 2026

3 Results

3.1 Conditions for suncup formation

Our time series highlight two distinct roughness regimes. The transition between regimes is marked by the onset of monotonically increasing vertical roughness indices, occurring on May 11th 2022, May 22nd 2023, and June 3rd 2024 for the three seasons, respectively (Fig. 1a-c). We refer to the period prior to these thresholds as the smooth (or textured) phase, and to the period after as the rough phase.

During the smooth phase, the horizontal roughness index ($\sigma_{\Delta CL}$) shows large variability, while vertical roughness indices (z_0 and RMSH) remain comparatively stable. In detail, $\sigma_{\Delta CL}$ peaks up to 250 mm, whereas z_0 and RMSH change by no more than 4 mm across all years (Fig. 1a-f). Here, isolated peaks in $\sigma_{\Delta CL}$ are decoupled from any vertical roughness signal and are often correlated with wind gusts (Fig. 1d-f, m-o). This suggests that wind-driven (dry) snow redistribution processes of surface erosion or deposition alter the horizontal structure of the snow surface, in agreement with previous findings from Amory et al. (2017). During the rough phase, this pattern reverses. Vertical roughness indices increase steeply and reach values one order of magnitude above the smooth baseline. Across all years, z_0 and RMSH change by up to 15 and 30 mm. Conversely, horizontal roughness flattens to a near-zero trend, with $\sigma_{\Delta CL}$ shrinking down to only 8 mm. The absence of a wind signature in $\sigma_{\Delta CL}$ during this phase suggests that suncup development, rather than wind redistribution, governs the evolution of surface roughness: in this phase, the surface is mostly a melt-refreeze crust, therefore rather insensitive to wind redistribution processes. In the following, we focus on the rough phase, which coincides with the snow ablation season and where suncup growth is the dominant surface degradation mechanism at our site.

By combining roughness time series with meteorological forcings and snowpack state variables, we define a set of conditions for the onset of suncup growth. The disappearance of cold content provides the first signal for roughness-prone conditions (Fig. 1g-i). Once it reaches zero for the first time, the snowpack is isothermal and can thereon melt and refreeze, initiating the first melt-related surface reliefs such as melt-refreeze crusts and ice layers. Then, the snowpack undergoes several melt-refreeze cycles, and the wetting front propagates until the bottom of the snowpack, with increasing average liquid water content (LWC, Fig. 1g-i)). The average daily snow surface temperature (TSS) progressively increases, together with the number of isothermal surface hours per day (Fig. 1j-l). Across all years, the transition from smooth to rough regime consistently occurs when TSS remains at 0°C for approximately 20 hours/day, with average snowpack LWC around 2%. This suggests that the persistence of melt-prone conditions, rather than their episodic occurrence, is the key threshold for suncup growth. Moreover, in all years, the suncup growth onset coincides with reduced wind speeds with respect to the smooth phase, likely attributable to the seasonal shift in thermal conditions. With above-freezing air temperatures and high wind speeds, more heat is likely delivered to the suncups' ridges rather than the hollows, therefore reducing the deepening process. Together, these indicators mark favorable conditions for the onset of suncup growth: (1) a snowpack that has reached an isothermal state, (2) near-continuous daily surface melt, and (3) reduced wind speeds. As noted above, the smooth phase corresponds predominantly to the accumulation period, whereas the rough phase coincides with snowpack ablation and higher melt rates (Fig. 1p-r).

https://doi.org/10.5194/egusphere-2026-3049
Preprint. Discussion started: 3 June 2026

Figure 1. 2022 through 2024: (a-c) Vertical roughness indices, z_0 and RMSH; (d-f) Horizontal roughness index, expressed as the standard deviation of the difference between CL in both directions $\sigma_{\Delta CL}$; (g-i) SNOWPACK-simulated cold content (dark blue) and average snowpack liquid water content (light blue); (j-l) SNOWPACK-simulated snow surface temperature (blue) and the amount of isothermal surface occurrences per day (light red); (m-o) 3-h moving average of measured wind speeds; (p-r) measured snow depths (black) with accumulation and melt rates (light and dark blue, respectively).

https://doi.org/10.5194/egusphere-2026-3049
Preprint. Discussion started: 3 June 2026

3.2 Suncup dynamics across years

We observe suncups growing throughout the rough phase in all three years (Fig. 2a-c). Approximately 200 suncups formed every year over a 5x5 m survey sub-domain. The webcam and LiDAR acquisitions in Fig. 2a-f show that the 2D equivalent of the roughness coverage fraction η used in Larue et al. (2020) approaches 100% under natural conditions across all three seasons. The portions of the sub-domain not occupied by suncup hollows are, in fact, structured into ridges, leaving little to no flat reference area. This means that, under natural conditions, η alone cannot describe suncup development, motivating the use of additional descriptors.

During the initial two weeks of each rough phase, suncup growth is driven primarily by an increase in suncup number, after which individual features begin to merge and further growth is characterized by merging and deepening. Spring snowfall events periodically interrupted this progression, temporarily suspending suncup growth and producing abrupt decreases in depth and increases in size. Suncup growth is most pronounced in 2022, where depth and size reached peak values of approximately 30 mm and 10 cm, respectively, and depth growth rate was also considerably faster (Fig. 2m). This period was characterized by strong shortwave radiation gains and longwave losses, low relative humidity, and low wind speeds (Fig. 2p-x). Features were small, circular, and evenly distributed (Fig. 2d), consistent with the most favorable radiative and thermal conditions observed across the three years. In 2023, suncups developed at a slower pace, likely due to more persistent winds promoting turbulent heat exchange, and slightly lower net shortwave radiation in the initial phase compared to 2022. Nevertheless, favorable radiative conditions and dry air persisted, allowing suncups to reach considerable depths of 10 cm despite the slower growth rate (Fig. 2n,q,t). The persistent directional wind component also drove asymmetric ablation, resulting in notably larger, elongated features oriented along the prevailing NW wind direction, which remained consistent across the season ($\sigma = 51°$) (Fig. 2e,w). In 2024, conditions were the least favorable overall: substantially lower shortwave gains, high longwave gains due to frequent cloud cover, humid air, and high but highly variable wind speeds (Fig. 2r,u,x). On average, suncups in 2024 were 30% shallower than in 2022, with maximum depths reduced by 3 cm (Fig. 2o). The high directional variability of wind ($\sigma = 142°$) precluded the development of a preferred morphological axis despite the greatest total turbulent energy input across all three years, resulting in features less elongated than in 2023 (Fig. 2f). These observations suggest that suncup growth rate and depth are primarily governed by the radiative energy balance and modulated by humidity and wind speed, while suncup orientation and elongation are controlled by prevailing wind direction.

3.3 TARTES broadband albedo sensitivity to suncup growth and impurity loading

To determine the effect of suncups on the apparent broadband albedo, we compare measured time series with TARTES simulations in diffuse and direct illumination conditions for all years (Fig. 3a-f). We evaluate the quality of the simulations in dry and wet conditions separately (Fig. 3g-i), with wet conditions initiating when the daily average of the modelled LWC exceeded 1% on the top 30 cm (2022), or based on direct field measurements through 2023 and 2024 (Carletti et al., 2025). In smooth, dry conditions, the root mean squared error (RMSE) is 0.04 and the bias is on average -0.02 (diffuse) and -0.005 (direct); meaning that TARTES tends to slightly underestimate measured albedo on average, with random errors attributable to

https://doi.org/10.5194/egusphere-2026-3049
Preprint. Discussion started: 3 June 2026

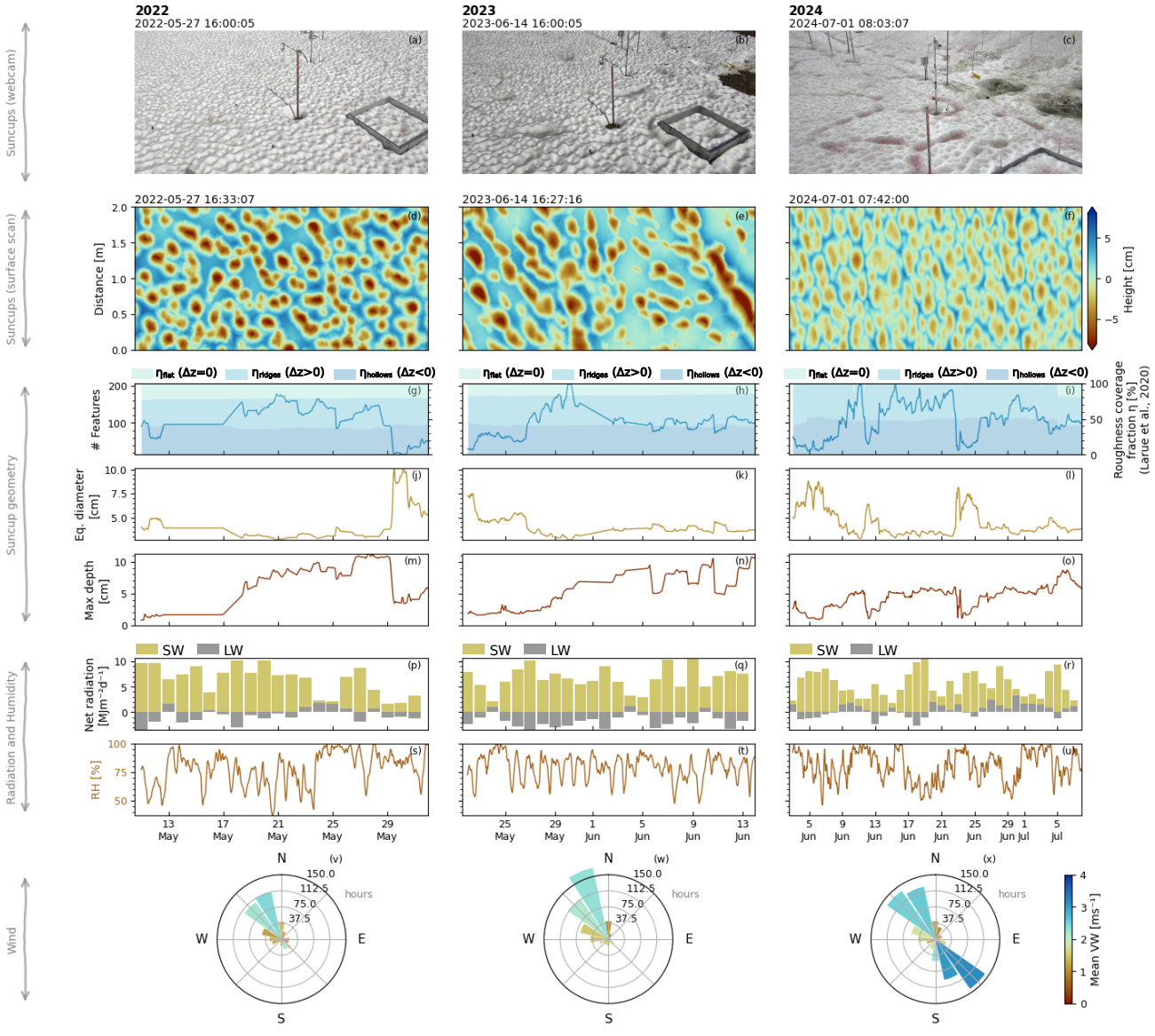

Figure 2. 2022 through 2024: (a-c) Suncups from webcam acquisitions next to the field of view of the LiDAR scanner. (d-f) Suncups from processed DSMs from LiDAR point clouds acquired at the same time of the webcam snapshots. (g-i) Number of suncup features (blue line) and cover fractions (shaded areas) computed as the 2D equivalent of Larue et al. (2020). Specifically, η_{ridges}, $\eta_{hollows}$ and η_{flat} denote the areal proportion of each surface type within the control area ($\eta_{ridges} + \eta_{hollows} + \eta_{flat} = 1$) and are classified by deviation from mean elevation: ridges ($\Delta z > 0$), hollows (($\Delta z < 0$) and flat ($\Delta z = 0$)). (j-l) Suncup mean equivalent diameter; (m-o) Suncup maximum depth; (p-r) Cumulative daily net radiation, shortwave (yellow) and longwave (grey). (s-u) Relative humidity. (v-x) Wind speeds and directions. Every hourly time series is smoothed with a 3-h moving average.

https://doi.org/10.5194/egusphere-2026-3049
Preprint. Discussion started: 3 June 2026

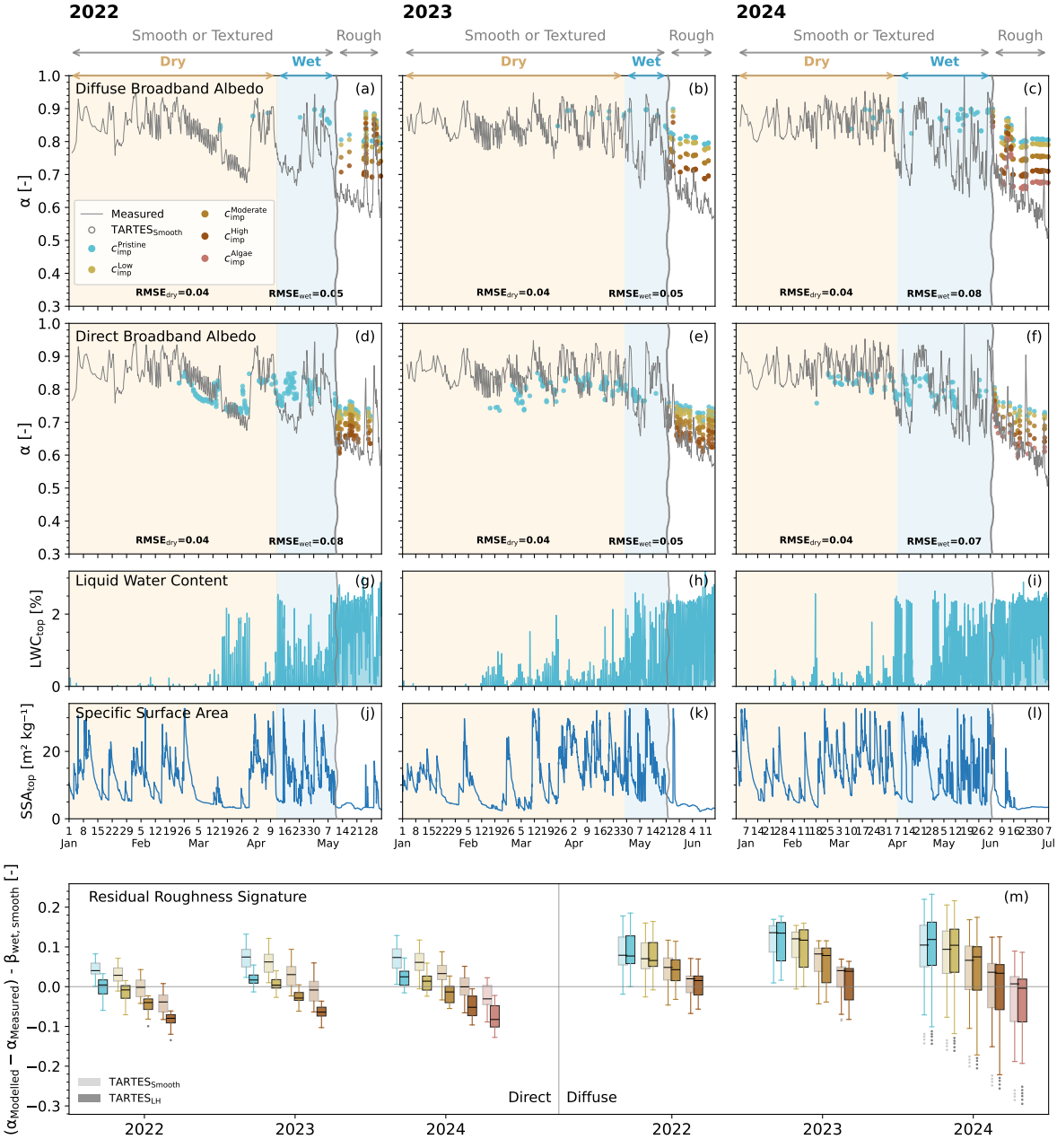

Figure 3. 2022 through 2024: (a-c) Measured and TARTES flat-surface broadband albedo for pristine and impurity-loaded snow under diffuse illumination conditions. (d-f) Measured and TARTES flat-surface broadband albedo for pristine and impurity-loaded snow under direct illumination conditions. (g-i) SNOWPACK-modelled liquid water content (LWC) averaged over the top 30 cm. (j-l) SNOWPACK-modelled specific surface area (SSA) averaged over the top 10 cm. (m) Residual roughness signatures in direct and diffuse illumination for pristine and impurity-loaded scenarios, comparing flat-surface TARTES simulations ($TARTES_{Smooth}$; transparent boxes) and TARTES corrected with the effective-albedo parametrization of Löwe and Helbig (2012) ($TARTES_{LH}$; opaque boxes).

https://doi.org/10.5194/egusphere-2026-3049
Preprint. Discussion started: 3 June 2026

minor forcing and model uncertainty. As the snow wets and SSA decreases, prior to suncup development, the overestimation of albedo in TARTES increases. The RMSE doubles up to roughly 0.08, with the bias turning strongly positive and contributing on average 70 and 50% of the RMSE in direct and diffuse conditions, respectively. We interpret this as the signal of wetting and metamorphism on a smooth surface ($\beta_{wet,smooth}$).

With the onset of suncup growth, we further partition the contributions to albedo reduction, and take into account the presence of impurities and algae on a wet, heavily metamorphosed snow. We quantify the suncup signature by subtracting $\beta_{wet,smooth}$ from the residual between measured and TARTES broadband albedo (Fig. 3m). On pristine snow, suncups generate albedo decreases of 0.05-0.12 and 0.09-0.15 for direct and diffuse conditions, respectively.

When accounting for low to medium impurity contents, the suncup signal becomes less important. Albedo decreases shrink down to 0.02-0.1 and 0.04-0.13 for direct and diffuse conditions, respectively. This suggests that roughness and impurities jointly contribute to the observed albedo deficit that TARTES cannot reproduce from optical properties alone. On the other hand, the suncup signal persists across most scenarios at the end of the season (Fig. 3a-f), suggesting that an even very high (assumed) impurity levels alone cannot explain the measured albedo decay. It is only for extremely high impurity contents or algal bloom that the suncup signal partially decouples from the impurity signal. In such cases, the suncup signal either only slightly persists or disappears (Fig. 3m). Considering all impurity contents in the rough regime, the bias explains the 76% of the RMSE on average, meaning that errors are non-random, and likely attributable to processes that are not represented in the model. The hypothesized algal cell concentration in 2024 brings albedo residuals below zero for direct illumination conditions, whereas albedo residuals converge to zero for diffuse conditions (Fig. 3m).

The effective albedo parametrization of Löwe and Helbig (2012) successfully reduces the residuals between measured broadband albedo and flat-surface TARTES simulations. The low-to-medium concentration range is the most probable at our site, and the residuals being closest to zero across all three years support this hypothesis. High impurity and algal bloom scenarios are, on the other hand, likely on the extreme side, and the fact that residuals fall below zero in such cases seems to support the hypothesis. As expected, under diffuse illumination, the parametrization either only marginally reduces the spread of residuals or converges towards the flat-surface results failing to fully capture the suncup signature, in contrast to its performance under direct illumination.

3.4 Impurity redistribution and suncup growth as interplaying controls on albedo decay

Fig. 4a shows that during the rough phase, the measured broadband albedo exhibits a strong logarithmic correlation with the aerodynamic roughness length z_0 ($\rho_s = -0.7$, $p = 10^{-40}$). Two categories of events deviate from this relationship: spring new snow layers depositing on pre-existing suncups, which progressively increase SSA and raise albedo above the fitted trend, and impurity loadings of exceptionally high magnitude, such as the 2024 algal bloom. The logarithmic fit further reveals that the rate of albedo decay is steepest at low z_0 and progressively relaxes as z_0 approaches values characteristic of deep suncups.

Two webcam acquisitions illustrating early-stage (Fig. 4b) and late-stage suncups (Fig. 4c) suggest a plausible mechanism underlying this behavior. At early stages, visible impurities are distributed relatively homogeneously across the snow surface. At late stages, despite likely higher total concentrations, impurities are preferentially concentrated in the hollows and, to a

https://doi.org/10.5194/egusphere-2026-3049
Preprint. Discussion started: 3 June 2026

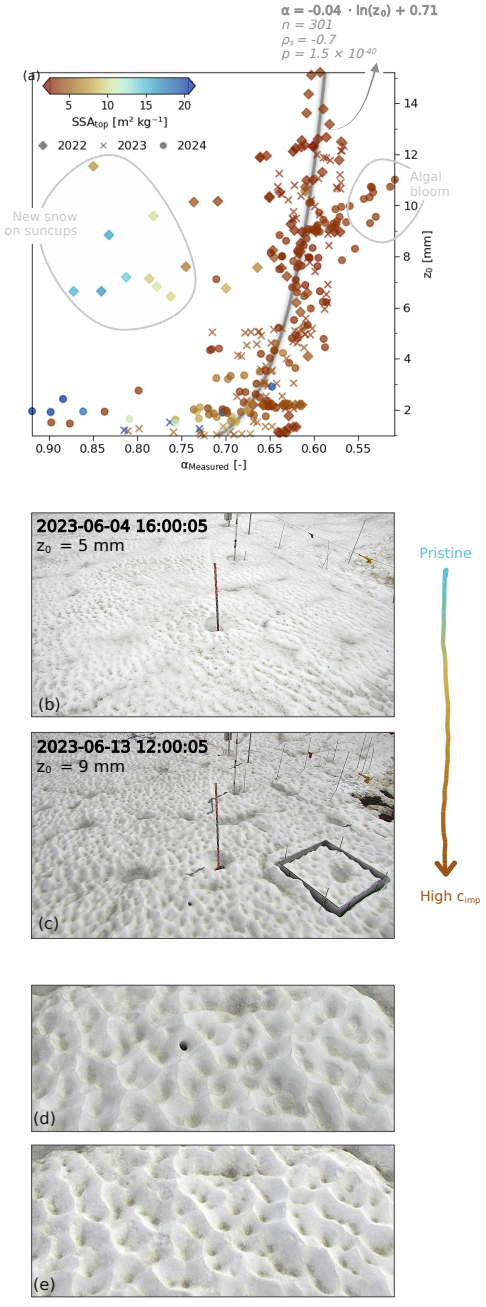

Figure 4. (a) KDE-averaged logarithmic correlation between measured broadband albedo α and aerodynamic roughness length z_0 across all years ($\alpha = -0.04 \cdot \ln(z_0) + 0.71$; $n = 301$; $\rho_s = -0.7$; $p = 10^{-40}$). The hourly data is resampled in a 3-h average. Outliers identify either thin new snow layers on the top of already developed suncups, or exceptionally high surface impurities, such as the 2024 algal bloom. (b) Webcam acquisition of early-stage suncups ($z_0 = 5$ mm). (c) Webcam acquisition of late-stage suncups ($z_0 = 9$ mm). (d,e) Detailed look at the differential distribution of impurities at suncups' hollows, ridges and walls.

https://doi.org/10.5194/egusphere-2026-3049
Preprint. Discussion started: 3 June 2026

lesser extent, at the ridges (Fig. 4d,e), leaving a greater proportion of the exposed snow surface comparatively clean. This redistribution pattern suggests that the coupling between suncup growth and impurity loading is most effective in driving albedo decay during the early-stage suncup phase. As suncups deepen, meltwater scavenges impurities into the hollows, likely attenuating the LAPs contribution to albedo decay, while the roughness effect becomes dominant. Taken together, these observations indicate that z_0 serves as a robust proxy for the combined albedo decay attributable to surface microtopography and impurity redistribution, integrating both effects regardless of their relative contributions at any given stage.

4 Discussion

Over three seasons of LiDAR monitoring of a snow surface, we have identified a smooth regime, characterized by dynamic horizontal roughness indices and relatively stable vertical roughness indices, and a rough regime, characterized by sharp increases in vertical roughness indices and steady horizontal roughness indices. These results confirm the findings of Fassnacht et al. (2023, 2009), who drew similar conclusions from only six observations across a single season. Our time series show that wind is the primary driver of horizontal roughness during the smooth regime (Fig. 1d-f, p-r): wind gusts coincide with sudden increases in horizontal roughness indices, while vertical roughness indices remain mainly unchanged. This suggests that wind-driven erosion and redistribution (producing features such as sastrugi and ripples) reorganize the snow surface laterally, extending the horizontal coherence of surface elements, without building comparable vertical reliefs. This confirms previous findings of Amory et al. (2017). The onset of the rough regime is marked by the formation of suncups. At our alpine latitude and altitude, we found that the conditions enabling suncup growth are the predominance of energy regimes allowing surface melting at lower wind speeds. These observations confirm that suncups lose mass through melting across their entire surface, including hollows, walls, and ridges, as described by Lliboutry (1954), and that their formation is driven by solar radiation (Matthes, 1934; Post and LaChapelle, 2000). Moreover, the fact that suncup initiation coincides with the daily preponderance of isothermal surface temperatures carries an important implication. As this threshold is easily detectable from both standard field sensors and snow simulations, it provides a simple diagnostic to detect the onset of suncups, opening the way for surface energy balance schemes to explicitly account for the transition from a flat to a rough surface regime during the ablation phase.

Our data show that the geometric arrangement of suncups varied substantially across years. In 2022 and 2023, clear-sky conditions likely favored radiation-driven suncup growth. Suncups reached shallower depths in 2023, likely due to more persistent winds delivering more turbulent energy to the ridges, and lower net shortwave radiation gains in the early formation phase. In 2024, overcast and windy conditions suggest a shift toward turbulent-dominated ablation, resulting in the shallowest suncups across all three years. Our observations are in agreement with the formation theories formulated by Matthes (1934); Lliboutry (1954); Mitchell and Tiedje (2010). Nevertheless, 2024 is an interesting case: suncups formed despite unfavorable radiative conditions. Although our data cannot confirm it, we offer the following hypothesis based on the framework of Rhodes et al. (1987). According to Rhodes et al. (1987), when ablation is dominated by turbulent heat exchange, impurities act as thermal insulators for snow, slowing melt where they are and allowing reliefs to deepen elsewhere. The threshold for this mechanism has been formalized in terms of dirt layer thickness (Tiedje et al., 2006; Betterton, 2001), though a quantitative threshold in

https://doi.org/10.5194/egusphere-2026-3049
Preprint. Discussion started: 3 June 2026

terms of impurity type or concentration remains unestablished. Exceptionally intense Saharan dust intrusions affected Switzerland in 2024 (Pons et al., 2025; Cuevas-Agulló et al., 2024), which, combined with prolonged melt duration and an unfrozen soil (Carletti et al., 2025) likely promoted the algal bloom visible in Fig. 2c (Roussel et al., 2024). Therefore, in 2024, the combination of dust and algal loading may have provided sufficient surface impurity concentration to trigger the turbulent formation regime described by Rhodes et al. (1987), enabling suncup development despite radiative conditions that would otherwise have caused their decay. We note, however, that Rhodes et al. (1987) assume impurities to be concentrated on ridges via the normal trajectory, whereas algae grow in-situ across the entire suncup surface, introducing uncertainty about whether their insulation feedback was fully active in 2024. This spatial distribution differs from the idealized scenario underlying the insulation feedback theory proposed by Rhodes et al. (1987). Whether the algal bloom was a necessary condition for suncup formation in 2024, or merely an enhancer of a transition primarily driven by meteorological forcing, cannot be determined from our observations alone.

We compared deviations of modelled broadband albedo from measurements against a baseline period where the snow surface was wet but suncups had not yet developed. This baseline accounts for two systematic biases inherent to TARTES under wet conditions. First, liquid water in snow triggers grain size growth through wet snow metamorphism and grain clustering (Brun, 1989). Optically, clustered grains behave as larger grains, increasing absorption and reducing albedo in comparison to dry snow. Second, TARTES relies on ice refractive indices neglecting the presence of liquid water. Although small, in the NIR regime there is an increase in the imaginary part of the refractive index from ice to liquid water (Green et al., 2006; Warren, 1982; O'Brien et al., 1981), which causes enhanced absorptions (Donahue et al., 2022; Dumont et al., 2017). Because TARTES does not account for the presence of liquid water in snow, the above neglected processes cause systematic overestimation of albedo during wet conditions that is independent of surface roughness. Similar observations were made by Manninen et al. (2021). By subtracting the bias for wet, smooth conditions from albedo residuals in the rough phase, we assume that these systematic errors are accounted for to the first order, leaving a signal that, in conditions of pristine snow, we can attribute to suncups and dirt accumulation alone.

Based on this and across all years, suncups cause broadband albedo decreases of 0.02–0.15 (Fig. 3m), in agreement with the results of Manninen et al. (2021) and slightly higher than the controlled experiments of Larue et al. (2020). Moreover, the albedo reduction is drastically accentuated in all years for values of SSA lower than 10 m^2kg^{-1} (Fig. 3j-l), as prescribed in Larue et al. (2020). These consistencies have two important implications. First, they provide independent field validation of previous experimental results: the albedo reductions documented by Larue et al. (2020) under artificially created roughness, and interpreted through a ray-tracing radiative transfer model, translate almost directly to natural suncup morphology observed over multiple melt seasons on Alpine snow. Second, it shows two apparent counterintuitive results that require discussion.

The first concerns the comparison with the study of Manninen et al. (2021), set in the Finnish tundra. The albedo reductions caused by deep Alpine suncups seem comparable to those caused by the shallower roughness features typical of tundra environments that Manninen et al. (2021) describe. Initially, this may indicate roughness coverage fraction, rather than feature depth, as the primary driver of albedo reduction. The study of Manninen et al. (2021) was conducted at 20° higher latitude than the Alps, where the sun elevation is systematically lower, i.e., solar zenith angles are larger at any time of day. Within the

https://doi.org/10.5194/egusphere-2026-3049
Preprint. Discussion started: 3 June 2026

theoretical framework of Larue et al. (2020), this first apparent contradiction is partially resolved: the authors demonstrate that an increase in suncup roughness coverage (at constant depths) causes significant albedo reductions, and that this is further amplified at large solar zenith angles through the effective-angle effect. In other words, the tundra roughness features of Manninen et al. (2021) may benefit from a stronger effective-angle contribution that may partially compensate for their shallower geometry, bringing their net albedo reduction into agreement with the deeper but differently illuminated alpine suncups. However, the possibility that coverage fraction is the dominant control deserves further investigation.

The second apparent contradiction concerns the illumination regime dependence of the roughness and impurity signal. The gap between measured and modelled albedo attributable to suncups and impurities is systematically larger under diffuse than under direct illumination. This seems to conflict with Warren et al. (1998), as direct illumination activates both multiple reflections and the effective-angle effect, whereas under diffuse illumination multiple reflections operates alone. Therefore, a stronger signal under diffuse conditions may seem counterintuitive at first. This result can be explained by several concurring factors. First, under direct illumination TARTES reduces albedo with increasing solar zenith angle, as oblique incidence enhances forward scattering; under diffuse illumination, angular effects are averaged into a single fixed hemispherically integrated value, leaving the model insensitive to any further geometry-driven albedo reduction. Second, our $\theta_s < 60°$ filter excludes the large solar zenith angle regime where the effective-angle effect is strongest (Larue et al., 2020), dampening the detectable roughness signal under direct illumination. Third, although suncups show preferential orientation along the main wind direction in one season (Fig. 2e), individual suncups maintain an isotropic periodic structure, reducing the relative importance of effective-angle effects (Painter and Dozier, 2004; Warren et al., 1998). Fourth, under diffuse illumination radiation arrives from the full sky hemisphere, meaning a geometrically larger fraction of photons enter suncups at oblique angles, i.e., the condition that maximizes internal reflections before escape. Thus, even though total incoming global radiation is substantially lower under overcast conditions, the fraction of intercepted photons undergoing multiple reflections may be larger under diffuse illumination. Bair et al. (2022) and Warren et al. (1998) both indicate that intermediate values of snow albedo, characteristic of rough ablation phases, are dominated by the multiple reflections effect. Moreover, Larue et al. (2020) quantified a strong multiple reflection effect precisely for the SSA ranges modelled by SNOWPACK across all our observed rough seasons. However, natural suncups differ significantly from the artificial configurations of Larue et al. (2020), where uncarved areas remained flat and coverage fractions approached 60% at maximum. Natural suncup fields, being structured into ridges or hollows, leave little to no flat surface, so coverage fractions approach 100%, suggesting that the multiple reflection mechanism likely operates at its theoretical maximum under natural conditions. Multiple reflection effects may be particularly relevant in alpine suncup roughness regimes, where overcast conditions driven by frontal systems, föhn events, and orographic cloudiness are substantially more frequent than in the predominantly clear-sky environment of the Sierra Nevada studied by Bair et al. (2022), though this remains a hypothesis that our data cannot directly confirm.

The dependence of the suncup signal on the illumination regime is further supported by the contrasting performance of the Löwe and Helbig (2012) effective albedo parametrization under direct and diffuse conditions. Despite being originally formulated to account for subgrid topographic shading, terrain reflections and limited sky view in large-scale models, this approach can be applied to smaller suncup geometries showing similar roughness feature characteristics. Under direct illumination, the

https://doi.org/10.5194/egusphere-2026-3049
Preprint. Discussion started: 3 June 2026

shading factor and mean-squared slope capture the effective angle effect very well, successfully reducing model residuals across all years. Under diffuse illumination, however, the shading factor vanishes by definition and the only remaining roughness correction is the redistribution of irradiance between sky and terrain fractions through the sky-view factor. This single exchange does not capture subsequent multiple reflections, causing the parametrization to converge toward flat-surface TARTES values and leaving the multiple reflections effect under diffuse conditions unaccounted for. This is particularly relevant in the presence of LAPs, where each subsequent reflection carries an increased probability of absorption.

The systematic co-existence of enhanced LAPs concentration and suncup growth has been addressed by our study, but remains a clear limitation of our modeling approach. The presence and evolution of impurities is not accounted for in SNOWPACK, which therefore neglects the enhanced SSA decrease derived from LAP-accelerated metamorphism (Skiles and Painter, 2019; Tuzet et al., 2017). Since we had no measurements of impurity content at our site, the scenarios we defined rely on literature values available for LAPs concentrations on seasonal Alpine snow. Specifically, our medium black carbon concentration matches the highest value measured in the two-seasons campaign of Tuzet et al. (2020), and is consistent with previous assessments in the Alps and beyond (Kau et al., 2026; Gabbi et al., 2015; Doherty et al., 2013; Painter et al., 2012). These campaigns included the melting season, when impurities that are not scavenged through percolating meltwater accumulate at the surface through melt amplification. This process can increase surface impurity concentrations by up to a factor of 5 (Doherty et al., 2013). This motivated our high black carbon scenario threshold, which is 5 times the low scenario. Dust carries greater uncertainty due to its even scarcer monitoring (Tuzet et al., 2020). We based our thresholds on the measurements and simulations of Di Mauro et al. (2019), despite the large-scale distribution assessment of Dumont et al. (2023) showing that dust deposition is strongly skewed towards the western Alps, likely making the high dust scenario unrealistic for our site. For the algal bloom scenario, we adopted the optical properties measured by Chevrollier et al. (2023) and the minimum bloom concentration detectable by Sentinel-2 from Roussel et al. (2024). These assumptions carry uncertainties that we are unable to quantify: the optical properties of Chevrollier et al. (2023) were estimated in an Arctic environment, where pigment content, cell size and packaging effects of the same species may differ; and the detection threshold of Roussel et al. (2024) is likely an overestimate of the minimum bloom concentration, especially given their finding that algal blooms seem more intense in the western rather than in the eastern Alps. Moreover, for all impurity types, the mass absorption efficiency must be assumed known, introducing further uncertainties (e.g., Tuzet et al. (2019)). Despite these limitations, the black carbon concentrations in our low and medium scenarios bracket the entire elemental carbon range reported by Manninen et al. (2021), and the corresponding roughness-induced albedo reductions are consistent with their findings, with a slight low bias attributable to the simultaneous presence of dust in our scenarios.

The measurements of Tuzet et al. (2017) show that surface LAPs concentrations follow a trend fully consistent with the suncup growth documented in this study. However, they also reveal no consistent inter-annual trend and, in agreement with Dumont et al. (2017), reveal significant scatter between measurement techniques. This suggests that increased measurement frequency alone would not straightforwardly resolve the suncups–LAPs disentanglement problem. A further complication arises from the fact that suncups favor differential LAPs concentration between hollows and ridges (Rhodes et al., 1987), meaning that a rigorous partitioning of their respective contributions to albedo decay would require tracking both suncup

https://doi.org/10.5194/egusphere-2026-3049
Preprint. Discussion started: 3 June 2026

geometry and LAPs distribution at the same fine spatial resolution. In the absence of tools capable of tracking surface LAPs evolution spatially and temporally and including their high-resolution vertical distribution in the surface snow (whether through distributed measurements or coupled models), this remains a fundamental obstacle to overcome in future.

The robust logarithmic relationship we identified between broadband albedo and aerodynamic roughness length (Fig. 4a) provides a physically informed proxy that helps address several open questions raised in this discussion. First, the partial decoupling of albedo decay from suncup growth during the pronounced algal bloom of 2024 suggests that in previous years, impurity concentrations either followed suncup growth closely enough to preserve the correlation, or remained too low to produce a detectable independent effect on albedo. Second, the logarithmic form of the correlation implies that albedo decays more rapidly at lower values of aerodynamic roughness length. The webcam imagery in Fig. 4b,c shows that, despite surface impurity concentrations likely being lower early in the ablation phase, impurities appear more evenly distributed across the surface of early-stage suncups. Later in the ablation phase, higher concentrations are progressively scavenged into the deepest sections of each suncup, with a small fraction persisting on the ridges (Fig. 4d,e). We propose that an even distribution of impurities over early-stage suncups produces a comparatively stronger effect on albedo decay: with the multiple-reflection effect operating at its maximum efficiency and the uniform distribution of absorbing particles, the probability of absorption at each reflection further increases. As the season progresses, albedo decay dampens likely because impurities, although present at higher concentrations, are scavenged into very localized sections of the suncups and become less homogeneously distributed. It is therefore possible that their radiative effect is dampened, despite higher bulk concentrations. This interpretation would provide another explanation on why the albedo reduction observed by Manninen et al. (2012) over shallower tundra suncups is comparable to that measured over our deeper alpine suncups, and it would support the hypothesis that coverage fraction has a stronger control on albedo decay than feature depth. This interpretation offers a physical explanation of the albedo decay intensity as the result of the interplay between roughness and impurities. However, our results alone can only suggest this without providing direct proof. The findings of Bair et al. (2022) highlight a fundamental measurement difficulty: spectroradiometry cannot distinguish the radiative effects of suncups from those of impurities in heterogeneous snow composed of mixed pristine and dirty fractions. Since this appears to be the dominant condition for suncup surfaces, it indirectly supports the use of our roughness proxy as an integrative measure of both effects.

These findings open concrete possibilities for improved remote sensing of snow surface properties and their representation in energy balance models. First, within the radiative footprint of a broadband pyranometer, suncup coverage is considerably easier to monitor than impurity concentration, and extremely more homogeneous spatially than the combined variability of multiple impurity types that are increasingly scavenged and redistributed. The identified correlation may therefore offer a practical approach to the LAPs quantification problem at the pyranometer footprint scale, and could be incorporated into snow energy balance models to simultaneously correct reflected shortwave radiation to account for both surface roughness and impurity effects. Second, the hypothesis that the coupling between suncup growth and impurity loading is most effective in driving albedo decay during the early-stage suncup phase would have direct implications for remote sensing in the ablation season. Because C-band radar backscatter over wet snow is highly sensitive to the early development of suncup roughness (Carletti

https://doi.org/10.5194/egusphere-2026-3049
Preprint. Discussion started: 3 June 2026

et al., 2025), these results highlight the potential value of assimilating surface roughness observations into snow energy balance models.

These findings open practical opportunities to improve both remote sensing of snow surface properties and their representation into snow energy balance models. First, within the radiative footprint of a broadband pyranometer, suncup coverage is considerably easier to monitor than impurity concentration, and spatially far more homogeneous than the combined variability of multiple impurity types undergoing scavenging and redistribution. The observed correlation may therefore provide a practical approach to the LAPs quantification at the pyranometer-footprint scale, and could be incorporated into snow energy balance models to simultaneously correct the reflected radiation to account for both suncup roughness and impurity effects. Second, if the coupling between suncup growth and impurity loading is most effective during the early stages of suncup development, this would have direct implications for radar observations throughout the ablation season. Because the C-band radar backscatter over wet snow is particularly sensitive to the early development of suncup roughness (Carletti et al., 2025), radar observations may offer a promising way to inform snow energy balance models on the evolving snow surface roughness and improve model representations of early-season albedo decay.

5 Conclusions

We monitored the formation and seasonal evolution of suncup roughness over three ablation seasons at a high-altitude alpine site. Suncup onset required a combination of sustained surface melting and low wind speeds. We identify the number of isothermal surface hours per day as a physically based indicator of suncup initiation, which is readily measurable with standard station instrumentation and could be used in energy balance models to flag the transition from flat- to rough-surface conditions. Across all three years, suncups consistently formed but with markedly different planar arrangements and geometry, which we explain through meteorological forcing and the formation regimes described in previous experimental work. However, whether suncups would have formed under turbulent-dominated conditions without the extreme impurity loadings of the 2024 algal bloom remains an open question. Comparing TARTES flat-surface simulations to broadband albedo measurements, we quantify the combined albedo decay attributable to suncups and surface impurities at 0.02–0.15, consistent with previous studies. Disentangling the two contributions is complicated by the fact that suncup growth and impurity surface enrichment follow similar seasonal trends, and by the extreme fine-scale heterogeneity of impurity distribution induced by suncup growth. A correct separation of the two effects would require simultaneous mapping of suncup geometry and impurity concentration at the same fine spatial scale. As a practical alternative, we identify a robust logarithmic correlation between measured broadband albedo and aerodynamic roughness length. Since roughness is considerably easier to monitor than fine-scale impurity content, this relationship could serve to correct reflected shortwave radiation in physical snow models, accounting for roughness and impurity effects simultaneously. The logarithmic form of the relationship also implies that albedo reduction is most intense at early stages of suncup development. We interpret this as the result of impurities being homogeneously distributed across the early-stage suncups before progressive melt scavenging concentrates them in localized sections, likely dampening their overall radiative effect. We hypothesize that the combination of early-stage roughness and evenly distributed impurities is more

https://doi.org/10.5194/egusphere-2026-3049
Preprint. Discussion started: 3 June 2026

efficient at reducing albedo than either factor acting alone. The C-band radar backscatter over wet snow is particularly sensitive to roughness at these early stages. If the co-occurrence of suncup initiation and impurity loading is indeed the dominant control on broadband albedo reduction, it represents a physically meaningful and remotely observable quantity that could be assimilated into energy balance snow models, directly addressing the need to account for surface roughness in snowpack energy balance computations.

Code and data availability. The dataset will be available on EnviDat: https://doi.org/10.16904/envidat.761. The code to reproduce the results will be available on GitHub.

Author contributions. FC: conceptualization, methodology, software, validation, formal analysis, investigation, data curation, visualization, project administration, writing – original draft, review and editing. NH: formal analysis, methodology, writing – review and editing. NW: methodology, writing – review and editing. LB: methodology, data curation. MB: funding acquisition, supervision, writing – review and editing. BW: software, resources, data curation, writing – review and editing. ML: funding acquisition, supervision, writing – review and editing.

Competing interests. Author Nora Helbig serves as an associate editor for this journal.

https://doi.org/10.5194/egusphere-2026-3049
Preprint. Discussion started: 3 June 2026

References

Amory, C., Gallée, H., Naaim-Bouvet, F., Favier, V., Vignon, E., Picard, G., Trouvilliez, A., Piard, L., Genthon, C., and Bellot, H.: Seasonal Variations in Drag Coefficient over a Sastrugi-Covered Snowfield in Coastal East Antarctica, Boundary-Layer Meteorology, 164, 107–133, https://doi.org/10.1007/s10546-017-0242-5, 2017.

Armstrong, R. L. and Brodzik, M. J.: Recent northern hemisphere snow extent: A comparison of data derived from visible and microwave satellite sensors, Geophysical Research Letters, 28, 3673–3676, https://doi.org/https://doi.org/10.1029/2000GL012556, 2001.

Bair, E. H., Dozier, J., Davis, R. E., Colee, M. T., and Claffey, K. J.: CUES—a study site for measuring snowpack energy balance in the Sierra Nevada, Frontiers in Earth Science, Volume 3 - 2015, https://doi.org/10.3389/feart.2015.00058, 2015.

Bair, E. H., Rittger, K., Davis, R. E., Painter, T. H., and Dozier, J.: Validating reconstruction of snow water equivalent in California's Sierra Nevada using measurements from the NASA Airborne Snow Observatory, Water Resources Research, 52, 8437–8460, https://doi.org/https://doi.org/10.1002/2016WR018704, 2016.

Bair, E. H., Dozier, J., Stern, C., LeWinter, A., Rittger, K., Savagian, A., Stillinger, T., and Davis, R. E.: Divergence of apparent and intrinsic snow albedo over a season at a sub-alpine site with implications for remote sensing, The Cryosphere, 16, 1765–1778, https://doi.org/10.5194/tc-16-1765-2022, 2022.

Bartelt, P. and Lehning, M.: A physical SNOWPACK model for the Swiss avalanche warning: Part I: numerical model, Cold Regions Science and Technology, 35, 123–145, https://doi.org/https://doi.org/10.1016/S0165-232X(02)00074-5, 2002.

Bavay, M. and Egger, T.: MeteoIO 2.4.2: a preprocessing library for meteorological data, Geoscientific Model Development, 7, 3135–3151, https://doi.org/10.5194/gmd-7-3135-2014, 2014.

Betterton, M. D.: Theory of structure formation in snowfields motivated by penitentes, suncups, and dirt cones, Phys. Rev. E, 63, 056 129, https://doi.org/10.1103/PhysRevE.63.056129, 2001.

Bond, T. C. and Bergstrom, R. W.: Light Absorption by Carbonaceous Particles: An Investigative Review, Aerosol Science and Technology, 40, 27–67, https://doi.org/10.1080/02786820500421521, 2006.

Brun, E.: Investigation on Wet-Snow Metamorphism in Respect of Liquid-Water Content, Annals of Glaciology, 13, 22–26, https://doi.org/10.3189/S0260305500007576, 1989.

Calonne, N., Richter, B., Löwe, H., Cetti, C., ter Schure, J., Van Herwijnen, A., Fierz, C., Jaggi, M., and Schneebeli, M.: The RHOSSA campaign: multi-resolution monitoring of the seasonal evolution of the structure and mechanical stability of an alpine snowpack, The Cryosphere, 14, 1829–1848, https://doi.org/10.5194/tc-14-1829-2020, 2020.

Caponi, L., Formenti, P., Massabó, D., Di Biagio, C., Cazaunau, M., Pangui, E., Chevaillier, S., Landrot, G., Andreae, M. O., Kandler, K., Piketh, S., Saeed, T., Seibert, D., Williams, E., Balkanski, Y., Prati, P., and Doussin, J.-F.: Spectral- and size-resolved mass absorption efficiency of mineral dust aerosols in the shortwave spectrum: a simulation chamber study, Atmospheric Chemistry and Physics, 17, 7175–7191, https://doi.org/10.5194/acp-17-7175-2017, 2017.

Carletti, F., Marin, C., Ghielmini, C., Bavay, M., and Lehning, M.: Multitemporal analysis of Sentinel-1 backscattering during snow melt using high-resolution field measurements and radiative transfer modeling, EGUsphere, 2025, 1–41, https://doi.org/10.5194/egusphere-2025-974, 2025.

Carroll, J. J.: The effect of surface striations on the absorption of shortwave radiation, Journal of Geophysical Research: Oceans, 87, 9647–9652, https://doi.org/https://doi.org/10.1029/JC087iC12p09647, 1982.

https://doi.org/10.5194/egusphere-2026-3049
Preprint. Discussion started: 3 June 2026

Chevrollier, L.-A., Cook, J. M., Halbach, L., Jakobsen, H., Benning, L. G., Anesio, A. M., and Tranter, M.: Light absorption and albedo reduction by pigmented microalgae on snow and ice, Journal of Glaciology, 69, 333–341, https://doi.org/10.1017/jog.2022.64, 2023.

Conway, H., Gades, A., and Raymond, C.: Albedo of dirty snow during conditions of melt, Water resources research, 32, 1713–1718, 1996.

Corbett, J. and Su, W.: Accounting for the effects of sastrugi in the CERES clear-sky Antarctic shortwave angular distribution models, Atmospheric Measurement Techniques, 8, 3163–3175, https://doi.org/10.5194/amt-8-3163-2015, 2015.

Corripio, J. G. and Purves, R. S.: Surface Energy Balance of High Altitude Glaciers in the Central Andes: The Effect of Snow Penitentes, chap. 3, pp. 15–27, John Wiley Sons, Ltd, https://doi.org/https://doi.org/10.1002/0470858249.ch3, 2005.

Cuevas-Agulló, E., Barriopedro, D., García, R. D., Alonso-Pérez, S., González-Alemán, J. J., Werner, E., Suárez, D., Bustos, J. J., García-Castrillo, G., García, O., Barreto, A., and Basart, S.: Sharp increase in Saharan dust intrusions over the western Euro-Mediterranean in February–March 2020–2022 and associated atmospheric circulation, Atmospheric Chemistry and Physics, 24, 4083–4104, https://doi.org/10.5194/acp-24-4083-2024, 2024.

Dadic, R., Mullen, P. C., Schneebeli, M., Brandt, R. E., and Warren, S. G.: Effects of bubbles, cracks, and volcanic tephra on the spectral albedo of bare ice near the Transantarctic Mountains: Implications for sea glaciers on Snowball Earth, Journal of Geophysical Research: Earth Surface, 118, 1658–1676, https://doi.org/https://doi.org/10.1002/jgrf.20098, 2013.

Di Mauro, B., Garzonio, R., Rossini, M., Filippa, G., Pogliotti, P., Galvagno, M., Morra di Cella, U., Migliavacca, M., Baccolo, G., Clemenza, M., Delmonte, B., Maggi, V., Dumont, M., Tuzet, F., Lafaysse, M., Morin, S., Cremonese, E., and Colombo, R.: Saharan dust events in the European Alps: role in snowmelt and geochemical characterization, The Cryosphere, 13, 1147–1165, https://doi.org/10.5194/tc-13-1147-2019, 2019.

Doherty, S. J., Grenfell, T. C., Forsström, S., Hegg, D. L., Brandt, R. E., and Warren, S. G.: Observed vertical redistribution of black carbon and other insoluble light-absorbing particles in melting snow, Journal of Geophysical Research: Atmospheres, 118, 5553–5569, https://doi.org/https://doi.org/10.1002/jgrd.50235, 2013.

Domine, F., Salvatori, R., Legagneux, L., Salzano, R., Fily, M., and Casacchia, R.: Correlation between the specific surface area and the short wave infrared (SWIR) reflectance of snow, Cold Regions Science and Technology, 46, 60–68, https://doi.org/https://doi.org/10.1016/j.coldregions.2006.06.002, 2006.

Donahue, C., Skiles, S. M., and Hammonds, K.: Mapping liquid water content in snow at the millimeter scale: an intercomparison of mixed-phase optical property models using hyperspectral imaging and in situ measurements, The Cryosphere, 16, 43–59, https://doi.org/10.5194/tc-16-43-2022, 2022.

Dumont, M., Arnaud, L., Picard, G., Libois, Q., Lejeune, Y., Nabat, P., Voisin, D., and Morin, S.: In situ continuous visible and near-infrared spectroscopy of an alpine snowpack, The Cryosphere, 11, 1091–1110, https://doi.org/10.5194/tc-11-1091-2017, 2017.

Dumont, M., Gascoin, S., Réveillet, M., Voisin, D., Tuzet, F., Arnaud, L., Bonnefoy, M., Bacardit Peñarroya, M., Carmagnola, C., Deguine, A., Diacre, A., Dürr, L., Evrard, O., Fontaine, F., Frankl, A., Fructus, M., Gandois, L., Gouttevin, I., Gherab, A., Hagenmuller, P., Hansson, S., Herbin, H., Josse, B., Jourdain, B., Lefevre, I., Le Roux, G., Libois, Q., Liger, L., Morin, S., Petitprez, D., Robledano, A., Schneebeli, M., Salze, P., Six, D., Thibert, E., Trachsel, J., Vernay, M., Viallon-Galinier, L., and Voiron, C.: Spatial variability of Saharan dust deposition revealed through a citizen science campaign, Earth System Science Data, 15, 3075–3094, https://doi.org/10.5194/essd-15-3075-2023, 2023.

Fassnacht, S., Williams, M., and Corrao, M.: Changes in the surface roughness of snow from millimetre to metre scales, Ecological Complexity, 6, 221–229, https://doi.org/https://doi.org/10.1016/j.ecocom.2009.05.003, special Section: Fractal Modeling and Scaling in Natural Systems, 2009.

https://doi.org/10.5194/egusphere-2026-3049
Preprint. Discussion started: 3 June 2026

Fassnacht, S. R., Suzuki, K., Sanow, J. E., Sexstone, G. A., Pfohl, A. K. D., Tedesche, M. E., Simms, B. M., and Thomas, E. S.: Snow Surface Roughness across Spatio-Temporal Scales, Water, 15, https://www.mdpi.com/2073-4441/15/12/2196, 2023.

Filhol, S. and Sturm, M.: Snow bedforms: A review, new data, and a formation model, Journal of Geophysical Research: Earth Surface, 120, 1645–1669, https://doi.org/https://doi.org/10.1002/2015JF003529, 2015.

Flanner, M. G., Shell, K. M., Barlage, M., Perovich, D. K., and Tschudi, M. A.: Radiative forcing and albedo feedback from the Northern Hemisphere cryosphere between 1979 and 2008, Nature Geoscience, 4, 151–155, https://doi.org/10.1038/ngeo1062, 2011.

Gabbi, J., Huss, M., Bauder, A., Cao, F., and Schwikowski, M.: The impact of Saharan dust and black carbon on albedo and long-term mass balance of an Alpine glacier, The Cryosphere, 9, 1385–1400, https://doi.org/10.5194/tc-9-1385-2015, 2015.

Green, R. O., Painter, T. H., Roberts, D. A., and Dozier, J.: Measuring the expressed abundance of the three phases of water with an imaging spectrometer over melting snow, Water Resources Research, 42, https://doi.org/https://doi.org/10.1029/2005WR004509, 2006.

Grenfell, T. C., Warren, S. G., and Mullen, P. C.: Reflection of solar radiation by the Antarctic snow surface at ultraviolet, visible, and near-infrared wavelengths, Journal of Geophysical Research: Atmospheres, 99, 18 669–18 684, https://doi.org/https://doi.org/10.1029/94JD01484, 1994.

Helbig, N., Löwe, H., Mayer, B., and Lehning, M.: Explicit validation of a surface shortwave radiation balance model over snow-covered complex terrain, Journal of Geophysical Research: Atmospheres, 115, https://doi.org/10.1029/2010jd013970, 2010.

Jahn, A. and Kłapa, M.: On the Origin of Ablation Hollows (Polygons) on Snow, Journal of Glaciology, 7, 299–312, https://doi.org/10.3189/S0022143000031063, 1968.

Kau, D., Greilinger, M., Vukićević, A., Bielecki, J., Kronlachner, L., and Kasper-Giebl, A.: Light-absorbing snow impurities: nine years (2016–2024) of snowpack sampling close to Sonnblick Observatory, Austrian Alps, The Cryosphere, 20, 1619–1633, https://doi.org/10.5194/tc-20-1619-2026, 2026.

Kokhanovsky, A. A.: Light penetration in snow layers, Journal of Quantitative Spectroscopy and Radiative Transfer, 278, 108 040, https://doi.org/https://doi.org/10.1016/j.jqsrt.2021.108040, 2022.

Kokhanovsky, A. A. and Zege, E. P.: Scattering optics of snow, Appl. Opt., 43, 1589–1602, https://doi.org/10.1364/AO.43.001589, 2004.

Lacroix, P., Legrésy, B., Langley, K., Hamran, S., Kohler, J., Roques, S., Rémy, F., and Dechambre, M.: In situ measurements of snow surface roughness using a laser profiler, Journal of Glaciology, 54, 753–762, https://doi.org/10.3189/002214308786570863, 2008.

Larue, F., Picard, G., Arnaud, L., Ollivier, I., Delcourt, C., Lamare, M., Tuzet, F., Revuelto, J., and Dumont, M.: Snow albedo sensitivity to macroscopic surface roughness using a new ray-tracing model, The Cryosphere, 14, 1651–1672, https://doi.org/10.5194/tc-14-1651-2020, 2020.

Lehning, M., Bartelt, P., Brown, B., Fierz, C., and Satyawali, P.: A physical SNOWPACK model for the Swiss avalanche warning: Part II. Snow microstructure, Cold Regions Science and Technology, 35, 147–167, https://doi.org/https://doi.org/10.1016/S0165-232X(02)00073-3, 2002.

Leroux, C. and Fily, M.: Modeling the effect of sastrugi on snow reflectance, Journal of Geophysical Research: Planets, 103, 25 779–25 788, https://doi.org/https://doi.org/10.1029/98JE00558, 1998.

Lettau, H.: Note on Aerodynamic Roughness-Parameter Estimation on the Basis of Roughness-Element Description, Journal of Applied Meteorology (1962-1982), 8, 828–832, http://www.jstor.org/stable/26174682, 1969.

Lhermitte, S., Abermann, J., and Kinnard, C.: Albedo over rough snow and ice surfaces, The Cryosphere, 8, 1069–1086, https://doi.org/10.5194/tc-8-1069-2014, 2014.

https://doi.org/10.5194/egusphere-2026-3049
Preprint. Discussion started: 3 June 2026

Libois, Q., Picard, G., France, J. L., Arnaud, L., Dumont, M., Carmagnola, C. M., and King, M. D.: Influence of grain shape on light penetration in snow, The Cryosphere, 7, 1803–1818, https://doi.org/10.5194/tc-7-1803-2013, 2013.

Libois, Q., Picard, G., Dumont, M., Arnaud, L., Sergent, C., Pougatch, E., Sudul, M., and Vial, D.: Experimental determination of the absorption enhancement parameter of snow, Journal of Glaciology, 60, 714–724, https://doi.org/10.3189/2014JoG14J015, 2014.

Lliboutry, L.: The origin of penitents, Journal of Glaciology, 2, 331–338, 1954.

Löwe, H. and Helbig, N.: Quasi-analytical treatment of spatially averaged radiation transfer in complex terrain, Journal of Geophysical Research: Atmospheres, 117, https://doi.org/https://doi.org/10.1029/2012JD018181, 2012.

Manninen, A.: Surface roughness of Baltic sea ice, Journal of Geophysical Research: Oceans, 102, 1119–1139, 1997.

Manninen, A.: Multiscale surface roughness description for scattering modelling of bare soil, Physica A: Statistical Mechanics and its Applications, 319, 535–551, https://doi.org/https://doi.org/10.1016/S0378-4371(02)01505-4, 2003.

Manninen, T., Anttila, K., Karjalainen, T., and Lahtinen, P.: Automatic snow surface roughness estimation using digital photos, Journal of Glaciology, 58, 993–1007, https://doi.org/10.3189/2012JoG11J144, 2012.

Manninen, T., Anttila, K., Jääskeläinen, E., Riihelä, A., Peltoniemi, J., Räisänen, P., Lahtinen, P., Siljamo, N., Thölix, L., Meinander, O., Kontu, A., Suokanerva, H., Pirazzini, R., Suomalainen, J., Hakala, T., Kaasalainen, S., Kaartinen, H., Kukko, A., Hautecoeur, O., and Roujean, J.-L.: Effect of small-scale snow surface roughness on snow albedo and reflectance, The Cryosphere, 15, 793–820, https://doi.org/10.5194/tc-15-793-2021, 2021.

Matthes, F. E.: Ablation of snow-fields at high altitudes by radiant solar heat, Eos, Transactions American Geophysical Union, 15, 380–385, https://doi.org/https://doi.org/10.1029/TR015i002p00380, 1934.

Mitchell, K. A. and Tiedje, T.: Growth and fluctuations of suncups on alpine snowpacks, Journal of Geophysical Research: Earth Surface, 115, https://doi.org/https://doi.org/10.1029/2010JF001724, 2010.

O'Brien, H., Koh, G., Research, C. R., (U.S.), E. L., and of Engineers, U. S. A. C.: Near-infrared Reflectance of Snow-covered Substrates, CRREL report, The Laboratory, https://books.google.ch/books?id=Sn0rBGC-EPMC, 1981.

Painter, T. H. and Dozier, J.: Measurements of the hemispherical-directional reflectance of snow at fine spectral and angular resolution, Journal of Geophysical Research: Atmospheres, 109, https://doi.org/https://doi.org/10.1029/2003JD004458, 2004.

Painter, T. H., Duval, B., Thomas, W. H., Mendez, M., Heintzelman, S., and Dozier, J.: Detection and Quantification of Snow Algae with an Airborne Imaging Spectrometer, Applied and Environmental Microbiology, 67, 5267–5272, https://doi.org/10.1128/AEM.67.11.5267-5272.2001, 2001.

Painter, T. H., Bryant, A. C., and Skiles, S. M.: Radiative forcing by light absorbing impurities in snow from MODIS surface reflectance data, Geophysical Research Letters, 39, https://doi.org/https://doi.org/10.1029/2012GL052457, 2012.

Picard, G. and Libois, Q.: Simulation of snow albedo and solar irradiance profile with the Two-streAm Radiative TransfEr in Snow (TARTES) v2.0 model, Geoscientific Model Development, 17, 8927–8953, https://doi.org/10.5194/gmd-17-8927-2024, 2024.

Picard, G., Dumont, M., Lamare, M., Tuzet, F., Larue, F., Pirazzini, R., and Arnaud, L.: Spectral albedo measurements over snow-covered slopes: theory and slope effect corrections, The Cryosphere, 14, 1497–1517, https://doi.org/10.5194/tc-14-1497-2020, 2020.

Pons, F. et al.: Assessing climate change impacts on the March 2024 compound floods and Saharan dust outbreak in Europe, Journal of Geophysical Research: Atmospheres, https://doi.org/10.1029/2024JD042218, 2025.

Post, A. and LaChapelle, E. R.: Glacier ice, University of Toronto Press, 2000.

Reindl, D., Beckman, W., and Duffie, J.: Diffuse fraction correlations, Solar Energy, 45, 1–7, https://doi.org/10.1016/0038-092x(90)90060-p, 1990.

https://doi.org/10.5194/egusphere-2026-3049
Preprint. Discussion started: 3 June 2026

Rhodes, J. J., Armstrong, R. L., and Warren, S. G.: Mode of Formation of "Ablation Hollows" Controlled by Dirt Content of Snow, Journal of Glaciology, 33, 135–139, https://doi.org/10.3189/S0022143000008601, 1987.

Richardson, W. E. and Harper, R. D. M.: Ablation Polygons on Snow—Further Observations and Theories, Journal of Glaciology, 3, 25–27, https://doi.org/10.3189/S0022143000024667, 1957.

Robledano, A., Picard, G., Dumont, M., Flin, F., Arnaud, L., and Libois, Q.: Unraveling the optical shape of snow, Nature Communications, 14, 3955, https://doi.org/10.1038/s41467-023-39671-3, 2023.

Roussel, L., Dumont, M., Gascoin, S., Monteiro, D., Bavay, M., Nabat, P., Ezzedine, J. A., Fructus, M., Lafaysse, M., Morin, S., and Maréchal, E.: Snowmelt duration controls red algal blooms in the snow of the European Alps, Proceedings of the National Academy of Sciences of the United States of America, 121, https://doi.org/10.1073/pnas.2400362121, 2024.

Ruttner, P., Voordendag, A., Hartmann, T., Glaus, J., Wieser, A., and Bühler, Y.: Monitoring snow depth variations in an avalanche release area using low-cost lidar and optical sensors, Natural Hazards and Earth System Sciences, 25, 1315–1330, https://doi.org/10.5194/nhess-25-1315-2025, 2025.

Schaepman-Strub, G., Schaepman, M., Painter, T., Dangel, S., and Martonchik, J.: Reflectance quantities in optical remote sensing—definitions and case studies, Remote Sensing of Environment, 103, 27–42, https://doi.org/https://doi.org/10.1016/j.rse.2006.03.002, 2006.

Schlögl, S., Lehning, M., and Mott, R.: How Are Turbulent Sensible Heat Fluxes and Snow Melt Rates Affected by a Changing Snow Cover Fraction?, Frontiers in Earth Science, Volume 6 - 2018, https://doi.org/10.3389/feart.2018.00154, 2018.

Skiles, S. M. and Painter, T. H.: Toward understanding direct absorption and grain size feedbacks by dust radiative forcing in snow with coupled snow physical and radiative transfer modeling, Water Resources Research, 55, 7362–7378, 2019.

Skiles, S. M., Flanner, M., Cook, J. M., Dumont, M., and Painter, T. H.: Radiative forcing by light-absorbing particles in snow, Nature Climate Change, 8, 964–971, https://doi.org/10.1038/s41558-018-0296-5, 2018.

Sommer, C. G., Lehning, M., and Fierz, C.: Wind Tunnel Experiments: Influence of Erosion and Deposition on Wind-Packing of New Snow, Frontiers in Earth Science, Volume 6 - 2018, https://doi.org/10.3389/feart.2018.00004, 2018.

Stewart, A., Rioux, D., Boyer, F., Gielly, L., Pompanon, F., Saillard, A., Thuiller, W., Valay, J.-G., Maréchal, E., and Coissac, E.: Altitudinal Zonation of Green Algae Biodiversity in the French Alps, Frontiers in Plant Science, Volume 12 - 2021, https://doi.org/10.3389/fpls.2021.679428, 2021.

Takahashi, S.: A study on ablation hollows on a melting snow surface, Low Temperature Science Series A,(37), 13, 1978.

Tapakis, R., Charalambides, A., and Michaelides, S.: Influence of Solar Altitude on Diffuse Fraction Correlations in Cyprus, in: Proceedings of the EuroSun 2014 Conference, EuroSun 2014, pp. 1–7, International Solar Energy Society, https://doi.org/10.18086/eurosun.2014.08.11, 2015.

Tiedje, T., Mitchell, K. A., Lau, B., Ballestad, A., and Nodwell, E.: Radiation transport model for ablation hollows on snowfields, Journal of Geophysical Research: Earth Surface, 111, https://doi.org/https://doi.org/10.1029/2005JF000395, 2006.

Tuzet, F., Dumont, M., Lafaysse, M., Picard, G., Arnaud, L., Voisin, D., Lejeune, Y., Charrois, L., Nabat, P., and Morin, S.: A multilayer physically based snowpack model simulating direct and indirect radiative impacts of light-absorbing impurities in snow, The Cryosphere, 11, 2633–2653, https://doi.org/10.5194/tc-11-2633-2017, 2017.

Tuzet, F., Dumont, M., Arnaud, L., Voisin, D., Lamare, M., Larue, F., Revuelto, J., and Picard, G.: Influence of light-absorbing particles on snow spectral irradiance profiles, The Cryosphere, 13, 2169–2187, https://doi.org/10.5194/tc-13-2169-2019, 2019.

https://doi.org/10.5194/egusphere-2026-3049
Preprint. Discussion started: 3 June 2026

Tuzet, F., Dumont, M., Picard, G., Lamare, M., Voisin, D., Nabat, P., Lafaysse, M., Larue, F., Revuelto, J., and Arnaud, L.: Quantification of the radiative impact of light-absorbing particles during two contrasted snow seasons at Col du Lautaret (2058 m a.s.l., French Alps), The Cryosphere, 14, 4553–4579, https://doi.org/10.5194/tc-14-4553-2020, 2020.

Vionnet, V., Brun, E., Morin, S., Boone, A., Faroux, S., Le Moigne, P., Martin, E., and Willemet, J.-M.: The detailed snowpack scheme Crocus and its implementation in SURFEX v7.2, Geoscientific Model Development, 5, 773–791, https://doi.org/10.5194/gmd-5-773-2012, 2012.

Warren, S. G.: Optical properties of snow, Reviews of Geophysics, 20, 67–89, https://doi.org/https://doi.org/10.1029/RG020i001p00067, 1982.

Warren, S. G.: Can black carbon in snow be detected by remote sensing?, Journal of Geophysical Research: Atmospheres, 118, 779–786, https://doi.org/https://doi.org/10.1029/2012JD018476, 2013.

Warren, S. G. and Wiscombe, W. J.: A Model for the Spectral Albedo of Snow. II: Snow Containing Atmospheric Aerosols, Journal of Atmospheric Sciences, 37, 2734 – 2745, https://doi.org/10.1175/1520-0469(1980)037<2734:AMFTSA>2.0.CO;2, 1980.

Warren, S. G., Brandt, R. E., and O'Rawe Hinton, P.: Effect of surface roughness on bidirectional reflectance of Antarctic snow, Journal of Geophysical Research: Planets, 103, 25 789–25 807, https://doi.org/https://doi.org/10.1029/98JE01898, 1998.

Wever, N., Fierz, C., Mitterer, C., Hirashima, H., and Lehning, M.: Solving Richards Equation for snow improves snowpack meltwater runoff estimations in detailed multi-layer snowpack model, The Cryosphere, 8, 257–274, https://doi.org/10.5194/tc-8-257-2014, 2014.

Wever, N., Würzer, S., Fierz, C., and Lehning, M.: Simulating ice layer formation under the presence of preferential flow in layered snowpacks, The Cryosphere, 10, 2731–2744, https://doi.org/10.5194/tc-10-2731-2016, 2016.

Wiscombe, W. J. and Warren, S. G.: A Model for the Spectral Albedo of Snow. I: Pure Snow, Journal of Atmospheric Sciences, 37, 2712 – 2733, https://doi.org/10.1175/1520-0469(1980)037<2712:AMFTSA>2.0.CO;2, 1980.

Würzer, S., Wever, N., Juras, R., Lehning, M., and Jonas, T.: Modelling liquid water transport in snow under rain-on-snow conditions – considering preferential flow, Hydrology and Earth System Sciences, 21, 1741–1756, https://doi.org/10.5194/hess-21-1741-2017, 2017.

Zhang, W., Qi, J., Wan, P., Wang, H., Xie, D., Wang, X., and Yan, G.: An Easy-to-Use Airborne LiDAR Data Filtering Method Based on Cloth Simulation, Remote Sensing, 8, https://doi.org/10.3390/rs8060501, 2016.

Zhuravleva, T. B. and Kokhanovsky, A. A.: Influence of surface roughness on the reflective properties of snow, Journal of Quantitative Spectroscopy and Radiative Transfer, 112, 1353–1368, https://doi.org/https://doi.org/10.1016/j.jqsrt.2011.01.004, 2011.